UNIVERSITY OF Nebraska Lincoln

THE UNIVERSITY OF IOWA

KU THE UNIVERSITY OF KANSAS

MISSOURI S&T

LINCOLN UNIVERSITY MISSOURI

NICC NEBRASKA INDIAN COMMUNITY COLLEGE

University of Nebraska Omaha

University of Nebraska Medical Center

KU MEDICAL CENTER The University of Kansas

SMART Shear Keys for Multi-Hazards Mitigation of Diaphragm-Free Girder Bridges - Phase I

Genda Chen, PhD, PE
Professor and Robert W Abbett Distinguished Chair in Civil Engineering
Department of Civil, Architectural, and Environmental Engineering
Missouri University of Science and Technology

Xinzhe Yuan
PhD Candidate
Department of Civil, Architectural, and Environmental Engineering
Missouri University of Science and Technology

MISSOURI S&T

2020

MATC

**SMART Shear Keys for Multi-Hazards Mitigation of Diaphragm-Free Girder Bridges
- Phase I: Design and Characterization**

Genda Chen, Ph.D., P.E.
Professor and Robert W. Abbett
Distinguished Chair in Civil Engineering
Department of Civil, Architectural, and
Environmental Engineering
Missouri University of Science and
Technology

Xinzhe Yuan, Ph.D. Candidate
Department of Civil, Architectural, and
Environmental Engineering
Missouri University of Science and
Technology

A Report on Research Sponsored by

Mid-America Transportation Center

University of Nebraska–Lincoln

December 31, 2020

Technical Report Documentation Page

1. Report No. 25-1121-0005-132-1	2. Government Accession No.	3. Recipient's Catalog No.	
4. Title and Subtitle SMART Shear Keys for Multi-Hazards Mitigation of Diaphragm-Free Girder Bridges - Phase I: Design and Characterization		5. Report Date December 31, 2020	
		6. Performing Organization Code Missouri S&T	
7. Author(s) Genda Chen Xinzhe Yuan		8. Performing Organization Report No. 25-1121-0005-132-1	
9. Performing Organization Name and Address Center for Intelligent Infrastructure Department of Civil, Architectural, and Environmental Engineering Missouri University of Science and Technology 500 W. 16th St. Rolla, MO 65409-0810		10. Work Unit No. (TRAIS)	
		11. Contract or Grant No. 69A3551747107	
12. Sponsoring Agency Name and Address Mid-America Transportation Center 2200 Vine St. PO Box 830851 Lincoln, NE 68583-0851		13. Type of Report and Period Covered Final Report August 1, 2017 - December 31, 2020	
		14. Sponsoring Agency Code MATC TRB RiP No. 91994-19	
15. Supplementary Notes			

16. Abstract

Earthquakes and tsunamis caused significant damage to bridges. An inappropriate design of shear keys may cause the excessive movement of bridge superstructure due to insufficient load resistances or the undesirable damage of bridge substructure due to the overstrength of shear keys. Interior shear keys are mainly used in short to medium span highway bridges to restrain the excessive transverse movement of superstructures. A well-designed bridge shear key should restrain the movement of bridge superstructure, limit the force transferred to bridge substructure, and be easily replaceable to improve the resilience of the entire bridge structure. To achieve these objectives, a Sliding, Modular, Adaptive, Replaceable, and Two-dimensional (SMART) shear key is proposed to optimize a tradeoff of force and displacement in the bridge structure. A SMART shear key consists of three concrete modules and steel assembly accessories. The three concrete modules are made of steel fiber-reinforced concrete to increase the ductility of the shear key. SMART shear keys mainly utilize the sliding friction mechanism to restrain the movement of bridge superstructure. Seven SMART shear key specimens were tested to investigate their load-carrying capacity. Numerical simulation and theoretical analysis were also conducted to support the test results with in-depth understanding. Based on the experimental results, numerical simulation, and theoretical analysis, SMART shear keys can provide an equivalent load-carrying capacity to conventional resilient interior shear keys with ease to replacement once damaged. A backbone curve of SMART shear keys is proposed to implement the SMART shear key element in seismic analysis.

17. ORCID No. of each Researcher Genda Chen: 0000-0002-0658-4356		18. Distribution Statement	
19. Security Classif. (of this report) Unclassified	20. Security Classif. (of this page) Unclassified	21. No. of Pages 46	22. Price

Table of Contents

List of Figures

List of Tables

Acknowledgments

Disclaimer

The contents of this report reflect the views of the authors, who are responsible for the facts and the accuracy of the information presented herein. This document is disseminated in the interest of information exchange. The report is funded, partially or entirely, by a grant from the U.S. Department of Transportation's University Transportation Centers Program. However, the U.S. Government assumes no liability for the contents or use thereof.

Executive Summary

Earthquakes and tsunamis caused significant damage to bridge structures in recent years. Past reconnaissance indicated that inappropriate design of bridge shear keys caused the excessive movement of bridge superstructure due to insufficient load resistance or the undesirable damage of bridge substructure due to the overstrength of shear keys. These observations highlight the importance of the proper design of bridge shear keys that are widely used in short- to medium-span highway bridges to restrain the excessive transverse movement of superstructure. A well-designed bridge shear key should restrain the movement of bridge superstructure, limit the force transferred to bridge substructure, and be easily replaceable to improve the resilience of the entire bridge structure. To achieve these objectives, a novel Sliding, Modular, Adaptive, Replaceable, and Two-dimensional (SMART) shear key is proposed in this study. A SMART shear key consists of three concrete modules and their steel assembly accessories. The three concrete modules are made of steel fiber-reinforced concrete to increase the ductility of the SMART shear keys. SMART shear keys mainly utilize the sliding friction mechanism to restrain the movement of bridge superstructure. Seven SMART shear key specimens were tested to investigate their load-carrying capacity. Numerical simulation and theoretical analysis were also conducted to support the test results with in-depth understanding. Based on the experimental results, numerical simulation, and theoretical analysis, SMART shear keys can provide an equivalent load-carrying capacity to conventional resilient shear keys with ease to replacement once damaged. A backbone curve of SMART shear keys is proposed to implement the SMART shear key element in seismic analysis.

Chapter 1 Introduction

1.1 Research motivation

      Bridges are bottlenecks of ground transportation networks for infrastructure operation safety. Protection of bridges from severe damage induced by natural hazards like earthquakes and tsunamis is of essential importance. Particularly, sacrificial shear keys are used in bridge cap beams and abutments to provide necessary transverse support to the bridge superstructure under small to moderate natural hazards and service loads, but intentionally fail under severe hazards so the bridge substructure and foundations can be protected. Such sacrificial keys function like hazard fuse elements between the superstructure and substructure of bridges. However, field observations on bridge behaviors and failure modes after the 2005 Hurricane Katrina, 2008 Wenchuan Earthquake in China, and 2010 Maule Earthquake in Chile showed that conventional concrete shear keys and seismic bars may not function as designed (Luna *et al.*, 2006; Yen *et al.*, 2009, 2011a, 2011b). Some of the representative shear key failures are shown in Figure 1.1.

(a) Lateral movement of I-10 twin bridge, USA

(b) Chada bridge with no diaphragms, Chile

(c) Las Mercedes bridge and girder unseating at abutments, Chile

Figure 1.1 Observed performance of conventional bridge shear keys

During the 2010 offshore Maule Earthquake in Chile, the superstructure of several girder bridges rotated and displaced, causing the out-of-plane rupture of concrete girders, flexural damage to lateral restrainers, and the drop-off of spans (Chen *et al.*, 2010). The majority of bridge superstructure damage during earthquakes is associated with the ineffectiveness and failure of shear keys. As shown in Figure 1.1(a), a representative span of the I-10 bridge was displaced during the 2005 Hurricane Katrina since the bridge deck, girders, and two end diaphragms formed an upside-down cup (Chen *et al.*, 2005). As water rose, air was trapped under the deck, causing the bridge spans to float on the water and several girders of I-10 twin bridges to fall into the water. This finding was strongly supported by the fact that the nearby US11 highway bridge survived the storm surge since it was designed to let air escape through shallow girders and holes in the end diaphragms. Therefore, it is imperative to develop

diaphragm-free girder bridge with novel shear keys as indicated by the field reconnaissance reports on observed bridge damage.

<u>1.2 Research objectives and significance</u>

The main goal of this research is to prevent bridge superstructure from damage caused by shear key failures as previously mentioned. A novel concept of diaphragm-free girder bridges with Sliding, Modular, Adaptive, Replaceable, and Two-dimensional (SMART) shear keys is explored and developed. Each SMART shear key consists of three precast concrete modules arranged in an inverted L-shape that are horizontally and vertically post-tensioned on site with replaceable unbonded steel bars to form two wedged sliding surfaces. When installed next to a girder and anchored into its support, the key provides controllable lateral and vertical friction forces during natural hazards and regulates corresponding displacements over time. It is hypothesized that the above failure modes can be eliminated by balancing the force and displacement applied on the bridge superstructure. This report is mainly focused on the experimental characterization and computational modeling of SMART shear keys under pushover loads with an intent to study their load-displacement behaviors and understand their resistance to the movement of bridge superstructure. Based on the experimental and numerical results, simplified design equations of the SMART shear keys are given to help engineers determine the resistant forces of the keys in practice.

While conventional shear keys as a fuse are satisfactory to protect bridge substructure from damage during many earthquake events, SMART shear keys can uniquely retain the fuse function in protecting the superstructure from excessive displacement in addition to ensuring the safety of substructure. Furthermore, the use of SMART shear keys may allow the removal of diaphragms in girder bridges so that bridge superstructure does not float under tsunamis and

storm surges as otherwise evidenced in field reconnaissance mentioned above. Once successfully developed and implemented, diaphragm-free girder bridges with SMART shear keys can reduce or eliminate damage in bridge superstructure when subjected to earthquakes, tsunamis, hurricanes, and floods, and thus represent an innovative multi-hazards mitigation strategy for transportation infrastructure.

In addition to hazard mitigation, SMART shear keys can help address several contemporary issues in civil infrastructure. Two-dimensional (2D) shear keys can transform seismic technology into engineering for natural hazards. The adaptive feature of the keys' time-varying friction on two wedged sliding surfaces makes it possible to balance the lateral force and displacement of bridge girders during an extreme event. The precast modular devices can be assembled on site, facilitating the accelerated construction of bridges (Azizinamini and Gull, 2014). The sacrificial devices allow rapid replacement when damaged in the case of extreme events, contributing to the post-event recovery of infrastructure. In a broader context, safer bridges and replaceable keys contribute to a more sustainable and resilient transportation network.

Chapter 2 Design and Fabrication of SMART Shear Keys

As mentioned in Section 1.1, the SMART shear key consists of three precast concrete modules arranged in an inverted L-shape that are horizontally and vertically post-tensioned on site with replaceable unbonded steel bars to form two wedged sliding surfaces. The detailed design of SMART shear keys and fabrication of SMART shear key specimens are presented in this chapter. First, to design the novel SMART shear keys, existing studies and Caltrans design approach of seismic shear keys are introduced. Particularly, the experimental and theoretical studies of interior shear keys that function like the SMART shear keys are summarized. Second, based on the existing knowledge of seismic interior shear keys in bridge abutments and cap beams, details such as the dimension and the dowel bars of novel SMART shear keys are determined. Finally, the lab fabrication of the SMART shear keys is introduced.

2.1 Past studies and Caltrans Design Code

2.1.1 Exterior sacrificial shear keys

In the past, extensive experimental and theoretical studies have been conducted to investigate the performance of exterior sacrificial bridge shear keys as shown in Figure 1.1(b). Kottari *et al.* (2020) studied the typical non-isolated exterior shear keys in Figure 2.1 and proposed a new design that would prevent a sudden unpredictable diagonal shear failure of this type of shear keys. The new design allowed a more predictable failure mechanism governed by the horizontal sliding of the shear key. Han *et al.* (2017) conducted an experimental program to study the seismic behavior of reinforced concrete (RC) sacrificial exterior shear keys. The influence of reinforcement ratios and construction joint types on the performance of shear keys was studied. Two analytical models for predicting the force-displacement backbone curves of the exterior shear keys with sliding shear failure and sliding friction failure were developed to help

design the exterior shear keys of highway bridges. Silva *et al.* (2009, 2010) and Megally *et al.* (2002) studied the load transfer mechanism of shear keys and developed a shear-friction model and a strut-and-tie model to predict the performance of the exterior shear keys in bridge abutments. Bozorgzadeh *et al.* (2006) carried the experimental study of bridge exterior shear keys subjected to lateral loads. Given the experimental results, they developed a simplified model to predict the capacity of shear keys in sliding shear failure mode. Moreover, several recommendations were made for construction details.
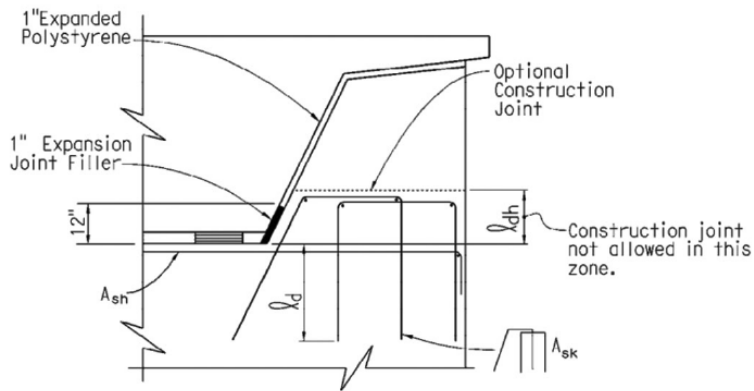
Figure 2.2 Non-isolated shear keys (Caltrans 2019)
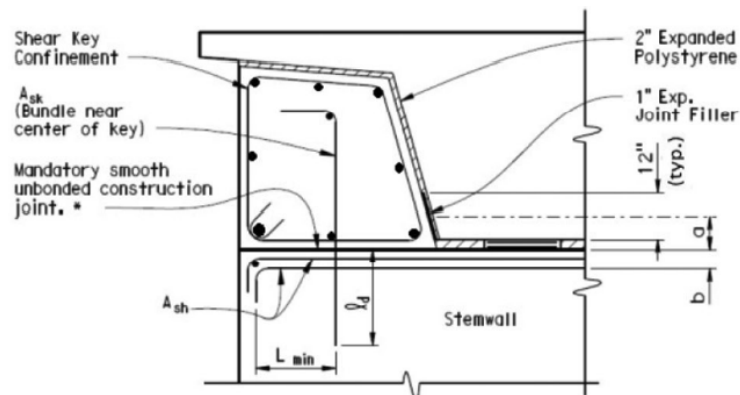
Figure 2.3 Isolated shear keys (Caltrans 2019)

Based on past studies, Caltrans seismic design code (Caltrans 2019) provided the design formulas of the two types of exterior shear keys in Figure 2.1 and Figure 2.2. Details of the exterior shear key design are referred to as the Caltrans Seismic Design Code.

2.1.2 Interior shear keys

Although there are extensive experimental and theoretical studies of the sacrificial exterior shear keys on bridge abutments, the results could not be directly applied to the design and fabrication of the new SMART shear keys because SMART shear keys are interior shear keys installed on the bridge cap beams and abutments to provide transverse support to the bridge superstructure. Unlike the exterior shear keys, there are limited studies of interior shear keys.

Han *et al.* (2018, 2020) studied the seismic capacity of interior shear keys for highway bridges, as shown in Figure 2.3. These interior shear keys are different from the exterior shear keys mainly because they are placed next to each bridge girder while the exterior shear keys are only placed at the two ends of the abutment or cap beam. The interior shear keys are commonly used to restrict the excessive transverse movement of the superstructures of short- to medium-span highway bridges under minor to moderate earthquake and service loads. Han *et al.* (2018, 2020) tested the seismic capacity of six interior shear key specimens with different main variables like the number of vertical bars, vertical bar ratio, hoop ratio, shear span ratio, loading height, and construction joint. Three failure modes of the six specimens were observed and different analytical models and an empirical formula were developed to estimate the resistant capacity of the shear keys.

(a) Abutment   (b) Cap beam
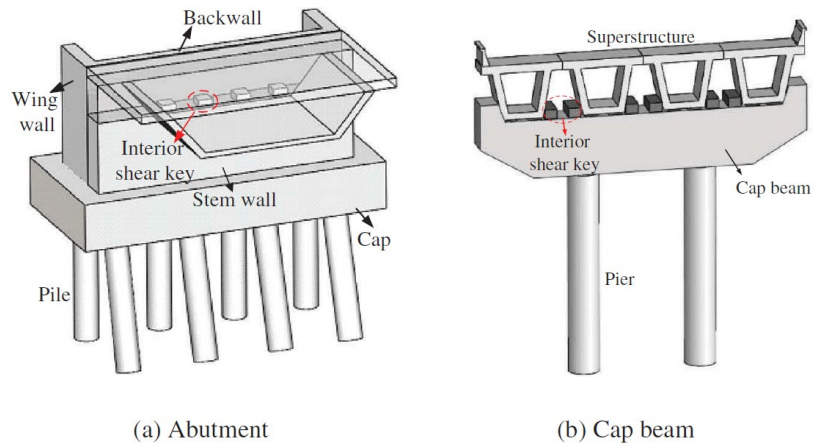
Figure 2.4 Interior shear keys in the abutment and cap beam of bridges (Han *et al.*, 2018, 2020)

The dimension of shear key specimens was 350×500×400 mm. The six specimens were divided into two groups: monolithic and resilient group shown in Figure 2.4, respectively. The main difference between the monolithic and resilient group is that for the resilient group, an artificial sliding interface was set between the shear key and stem wall via a kraft layer. Polystyrene foam blocks with a size of 88×80×30 mm were placed around the vertical reinforcement above the artificial sliding interface as shown in Figure 2.4(b). The resilient interior shear keys were expected to possess better ductility capacity than the monolithic shear keys.
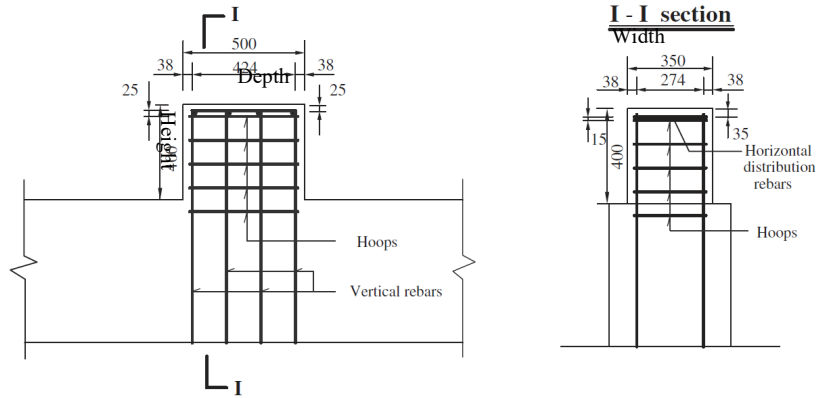
(d) Monolithic construction joint
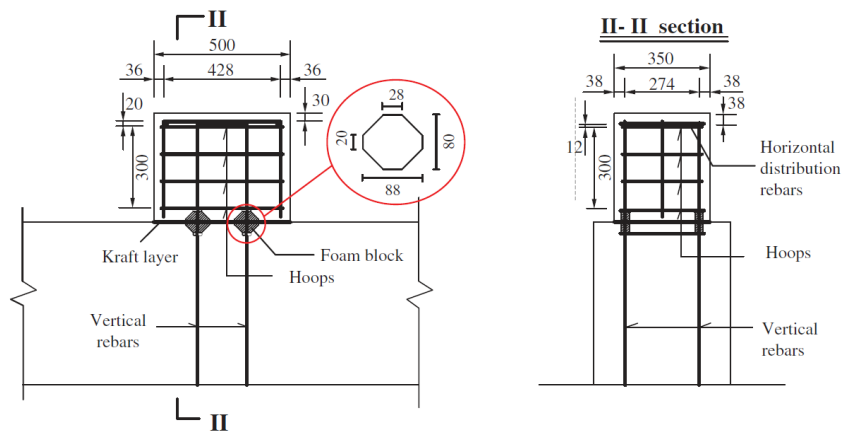
(e) Resilient construction joint

Figure 2.5 Monolithic and resilient types of interior shear keys (Han *et al.*, 2018, 2020)

The test results were summarized in Table 2.1. The three different failure modes were shown in Figure 2.5. It can be concluded from the table and figure that the monolithic shear keys have a much larger maximum loading capacity with less ductility than the resilient shear keys.

Table 2.1 Test results of the six interior shear key specimens (Han *et al.*, 2018, 2020)

Specimen	Shear span ratio	Vertical rebar ratio, %	Maximum capacity, kip (kN)	Displacement, in (mm)	Construction joint
S1	0.6	0.52	120.95 (538)	0.20 (5.1)	Monolithic
S2	0.4	0.52	167.94 (747)	0.12 (3.0)	
S3	0.2	0.52	200.99 (894)	0.15 (3.8)	
S4	0.2	0.26	29.23 (130)	1.6 (40.7)	Resilient
S5	0.2	0.52	58.23 (259)	1.94 (49.4)	
S6	0.2	0.78	78.24 (348)	1.51 (38.4)	
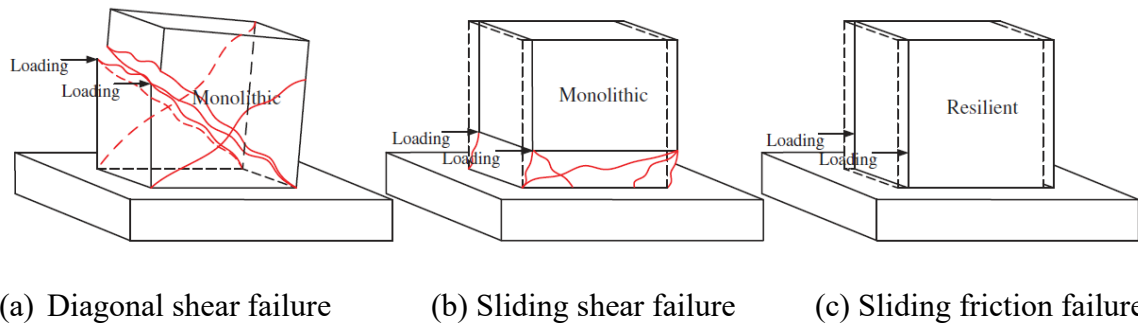
(a) Diagonal shear failure   (b) Sliding shear failure   (c) Sliding friction failure

Figure 2.6 Three failure models of the six shear key specimens (Han *et al.*, 2018, 2020)

The diagonal shear failure mode in Figure 2.5(a) includes a strut-and-tie mechanism. The maximum resistant load of the interior shear keys with the diagonal shear failure mode can be calculated from Equation 2.1

$$V_m = \frac{d}{2h_0} A_s f_m + \frac{1}{2} A_s^g f_s^g \qquad (2.1)$$

where A_s is the total area of vertical reinforcement; f_m is the ultimate tensile strength of vertical reinforcement; A_s^g is the total area of hoops; f_s^g is the ultimate tensile strength of hoops; d is the width of the shear key, and h_0 is the loading height.

For the sliding shear friction mechanism in Figure 2.5(b), the resistant capacity depended on the contribution of the vertical reinforcement and the friction of concrete. The ultimate capacity of the shear key with the sliding shear failure can be calculated from Equation 2.2

$$V_m = A_s f_m \left(\frac{\sqrt{\varepsilon_m^2 + 2\varepsilon_m}}{1 + \varepsilon_m} + \frac{\mu_1}{1 + \varepsilon_m} \right) \tag{2.2}$$

where $\varepsilon_m = 0.005$ is the ultimate strength of vertical reinforcement and $\mu_1 = 1.4$ is the kinematic coefficient of friction of rough concrete surface (Silva *et al.*, 2003).

For the sliding friction mechanism in Figure 2.5 (c), the resistant capacity depended on the bending of the vertical reinforcement and concrete friction. The ultimate capacity of the interior shear key with the sliding friction mechanism can be calculated from Equation 2.3

$$V_m = A_s f_m \left(\frac{\sqrt{\varepsilon_m^2 + 2\varepsilon_m}}{1 + \varepsilon_m} + \frac{\mu_2}{1 + \varepsilon_m} \right) \tag{2.3}$$

where $\mu_2 = 0.123$ is the kinematic coefficient of friction of a smooth concrete surface with kraft layer, which was obtained from the experimental results.

Silva *et al.* (2003) pointed out that existing design methodologies underestimated the maximum load-carrying capacity of sacrificial interior shear keys significantly, which could lead to severe inelastic strains in the piles. They studied a series of sacrificial interior shear keys that reflected typical proportions of interior shear keys in the state of California, as shown in Figure 2.3(a). These shear keys were cast in the stem wall with a monolithic construction joint, as

shown in Figure 2.4(a). In the Caltrans bridge design practice, shear keys were categorized based on their height-to-depth aspect ratio α, as shown in Figure 2.4 (a). When α < 0.5, the shear key capacity can be calculated using the shear friction model in Equation 2.4

$$V_m = \frac{A_s f_m}{\mu_1} \tag{2.4}$$

when $0.5 \leq \alpha \leq 1.0$, the shear key capacity can be calculated from the strut-and-tie model represented by Equation 2.5

$$V_m = \frac{A_s f_m}{\alpha} \tag{2.5}$$

when $1.0 < \alpha$, the shear key capacity can be calculated using the flexure beam model by Equation 2.6

$$V_m = \frac{j A_s f_m}{\alpha} \tag{2.6}$$

where j was assumed equal to 0.90. A concrete cracking strength model was adopted to calculate the capacity of the shear key by Equation 2.7

$$V_m = \frac{\pi}{2} f_{sp} b d \tag{2.7}$$

where f_{sp} is the concrete cylinder splitting strength, b is the width in Figure 2.4 (b), d is the depth in Figure 2.4 (a).

The test results showed that the maximum load-carrying capacity of all specimens was 235 kip (1045 kN), while the minimum capacity was 183 kip (814 kN) of the monolithic interior shear keys. The concrete cracking strength model generally generated the best estimation of shear key capacity among all analytical models.

2.2 Design of SMART shear keys

2.2.1 Design features of SMART shear keys

Following the previous discussion, the existing interior shear keys are mainly concrete teeth on bridge abutments or bridge cap beams with two types of construction joints: monolithic and resilient. Monolithic interior shear keys with severe damage due to lack of ductility cannot be used after an earthquake while resilient shear keys with slight damage after small earthquakes could be used after some limited repair. However, it will be much preferable if the damaged interior shear keys can be completely replaced after an earthquake or tsunami to maintain their design load-carrying capacities. Therefore, a novel SMART shear key as shown in Figure 2.6 is proposed to achieve the following design features:

Sliding When a girder pushes against the shear key vertically, Module I can slide against Module II to restrain and adapt to the vertical movement of the girder. The benefit of the sliding feature is to potentially increase the ductility of the interior shear key.

Modular Concrete blocks I, II, and III are precast with preserved holes. The anchor bolts are cast in the abutment or cap beam of a new bridge (or inserted and grouted in the hazard retrofit of an existing bridge in the future). The whole shear key system is assembled on site via dowel bars. The anchor bolts and vertical dowel bars are connected by steel couplers. The modular feature can facilitate the fabrication and installation of bridge interior shear keys compared to the cast concrete shear keys and end diaphragms.

Adaptive Due to the sliding feature, the SMART shear key can adjust to the lateral and vertical movements of the bridge girder, which can alleviate the pounding force between the girder and the shear key, further mitigating damage to structures.

Replaceable   The modular design of the SMART shear key makes it easier to replace once damaged in comparison with the cast-in-place concrete shear keys.

Two-dimensional   One main objective of the SMART shear key is to address the falling-girder problem observed in Interstate 10 Twin Span Bridge during the 2005 Hurricane Katrina. SMART shear keys can restrain the lateral and vertical movements of bridge girders to better prevent the bridge girders from falling off.
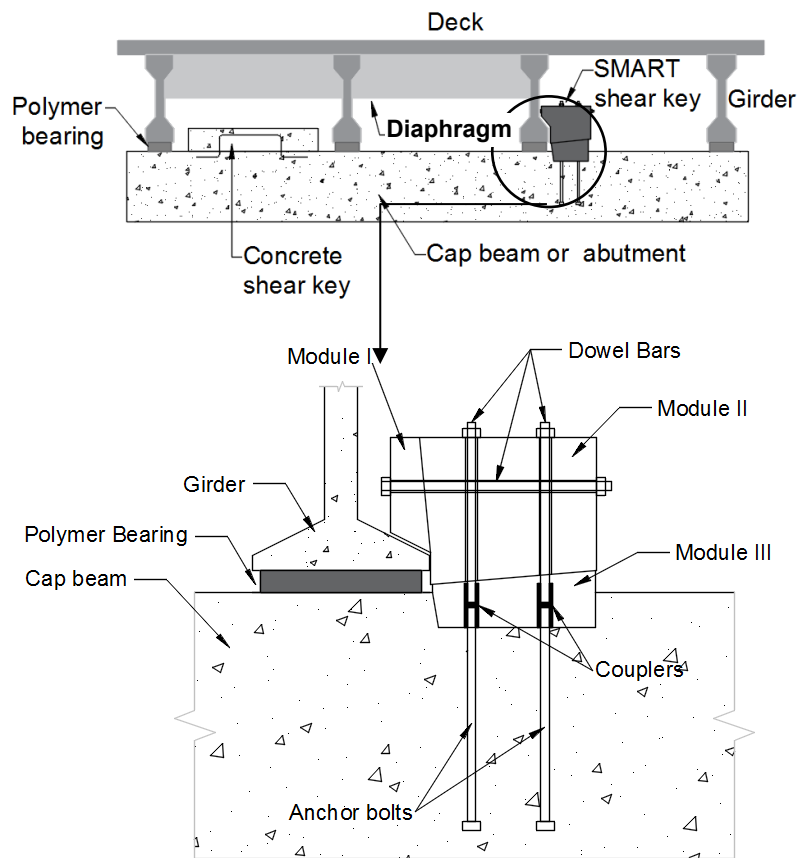
Figure 2.7 Schematic sketch of the concrete shear key and SMART shear keys

Module I, II, and III are concrete blocks. They are assembled by the dowel bars through the preserved holes in the concrete blocks. Between Module I and Module II there is a vertical

sliding interface. Likewise, a lateral sliding interface exists between Module II and Module III. The whole system is shown in Figure 2.6. The assembly of SMART shear keys is shown in Figure 2.7.
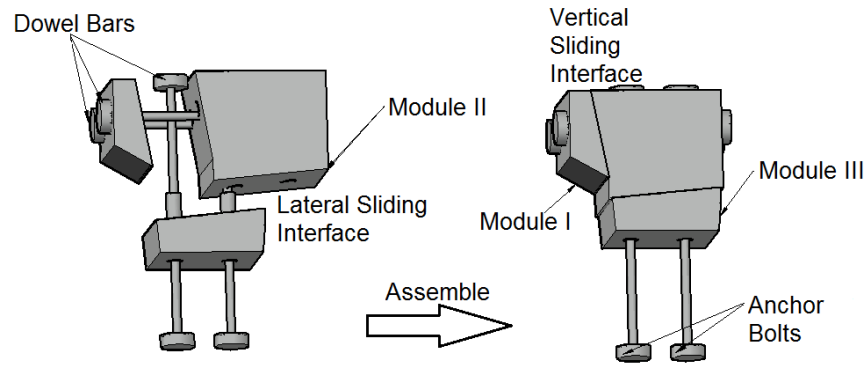
Figure 2.8 Assembling schematic diaphragm of a SMART shear key

2.2.2 Dimensions of SMART shear keys

As shown in Figure 2.6, the SMART shear keys are mainly designed for I-shape girder bridges. Therefore, the dimensions of SMART shear keys should fit the dimensions of an I-shape bridge girder. According to the LRFD Bridge Design Specification (AASHTO, 2014), the available standard I-beams have variable sizes such as beam depth, web thickness, and flange dimensions. The dimension of SMART shear keys can be designed based on the dimension of the target I-beam. For example, the contact interface between the I-beam flange and Module II of the SMART shear key should be designed such that the flange can be fitted to the contact surface. In this report, one design of SMART shear keys as shown in Figure 2.8 is studied to analyze its load-carrying capacity.
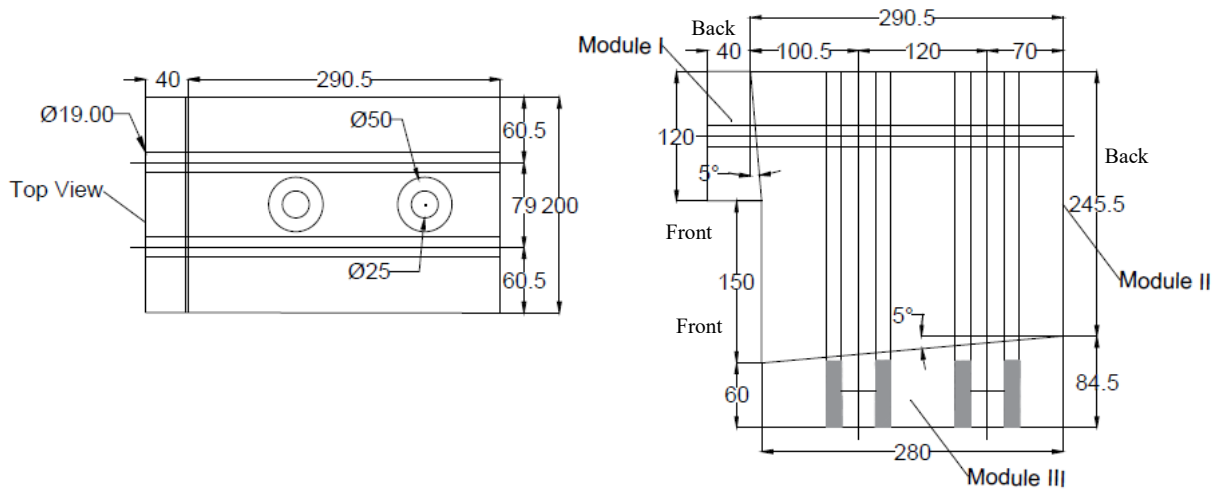
Figure 2.9 The dimension design of the SMART shear keys (mm)

The angles of the sliding interfaces between Module I and Module II and between Module II and Module III are both 5°. The vertical preserved holes on Module II and Module III have a diameter of 60 mm, which are originally determined by the size of couplers in Figure 2.6. The preserved horizontal holes on Module I and Module II can be determined by the horizontal dowel bars because there is no coupler in the horizontal direction to connect two bars together. As shown in Figure 2.8, in the direction of girders pushing the SMART shear keys, the front cover thickness of vertical dowel bars is 60 mm (around 2-3/8 in) while the back cover thickness of vertical dowel bars is 40 mm (around 1-1/2 in). The front and back cover thickness of horizontal dowel bars is around 60 mm. The purpose of using limited concrete cover is to make the SMART shear key as small as possible so that the heaviest Module II might be carried by a single person, which makes the installation of a replacement SMART shear key feasible because the interior shear keys are usually difficult to approach in practice. To compensate for the limited concrete cover, fiber-reinforced concrete is used to make the concrete modules of the SMART shear keys, which will be introduced in the next section.

16

2.3 Lab fabrication of SMART shear keys

2.3.1 Concrete modules

The concrete modules of the SMART shear key are made of plain concrete without steel reinforcement. Plain concrete could have high compressive strength but generally have very low tensile strength. The brittle plain concrete usually leads to a sudden failure of the shear key. Besides, the concrete cover thickness of dowel bars is relatively small, which further reduces the ductility of shear keys. Therefore, fiber-reinforced concrete is used to make SMART shear keys. Two types of steel fibers are used in this study, as shown in Figure 2.9.

(a) 1-inch steel fiber (25.4 mm)   (b) micro steel fiber
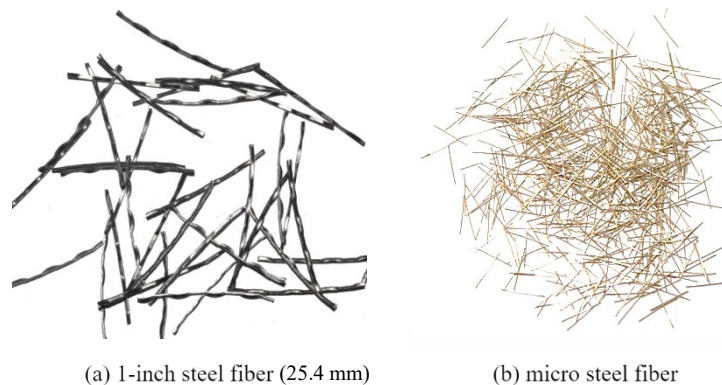
Figure 2.10 Two types of steel fibers

The fiber-reinforced concrete is mixed and used to cast the concrete modules as shown in Figure 2.10. Totally, seven smart shear keys were cast and tested. The first SMART shear key consisted of the long steel fibers as shown in Figure 2.9(a) while the remaining six shear keys consisted of the micro steel fibers due to the unavailability of long steel fibers in the lab. The first shear key was used for a trial to determine a reliable test plan to consecutively test one key after another. The remaining six shear keys were cast in two batches with three shear key molds as shown in Figure 2.10(a). The 28-day compressive strength of the shear key with long steel

fibers reaches 82 MPa (11.9 ksi). The 28-day compressive strength of the first three shear keys

batch with micro steel fibers reaches 64 MPa (9.3 ksi) and second batch reaches 68 MPa (9.9

ksi).

(a) Shear key molds (b) Fiber-reinforced concrete

(c) Shear key cast (d) Molds removal
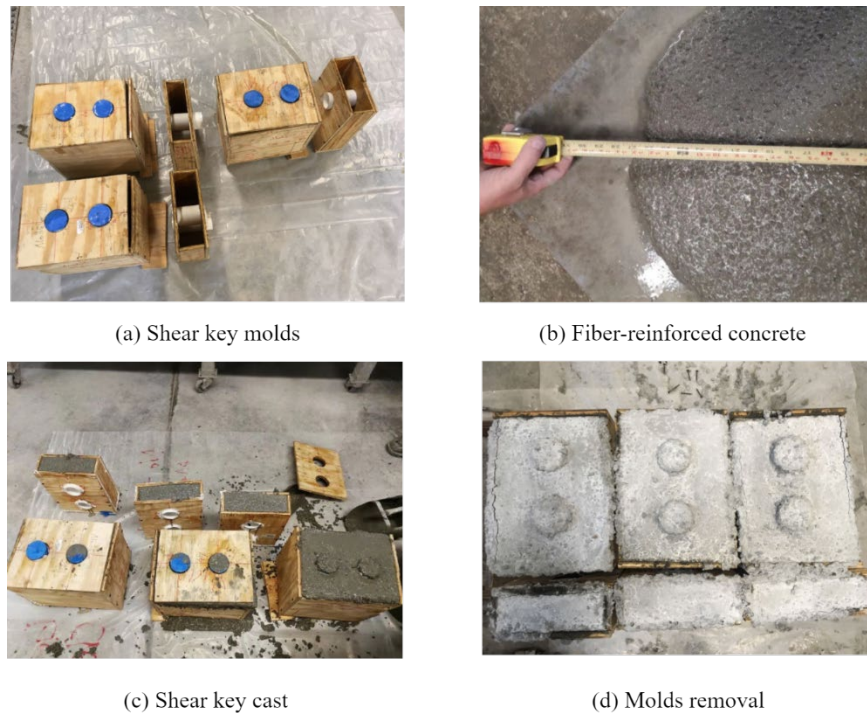
Figure 2.11 Casting of SMART shear keys

2.3.2 Installation accessories

In applications, the concrete modules are installed on the bridge abutments or cap beams

by steel threaded bars, couplers, hex nuts, and bearing plates, as shown in Figure 2.11. The

threaded bars are used as dowel bars to hold the concrete modules. The couplers are used to

connect two pieces of the threaded bars. Bearing plates and hex nuts are used to anchor the

whole shear key. These installation accessories were obtained from the Williams Form

Engineering Corp. The diameters of top dowel bars to hold the Concrete Module II are 25 mm (1

inch) and 19 mm (3/4 in), respectively. The diameter of the low anchor bars used in the cap beam is 32 mm (1-1/4 in). The strength of the dowel bars is Grade 75, 517 MPa (75 ksi). The strength of the anchor bars is 1034 MPa (150 ksi). The main purpose of using stronger anchor bars is to make sure the SMART shear key is safely installed. Corresponding couplers are used to connect the dowel bars and anchor bars with different diameters. After the concrete modules and installation accessories are prepared, the SMART shear keys are ready to be tested to study their loading-carrying capacity.
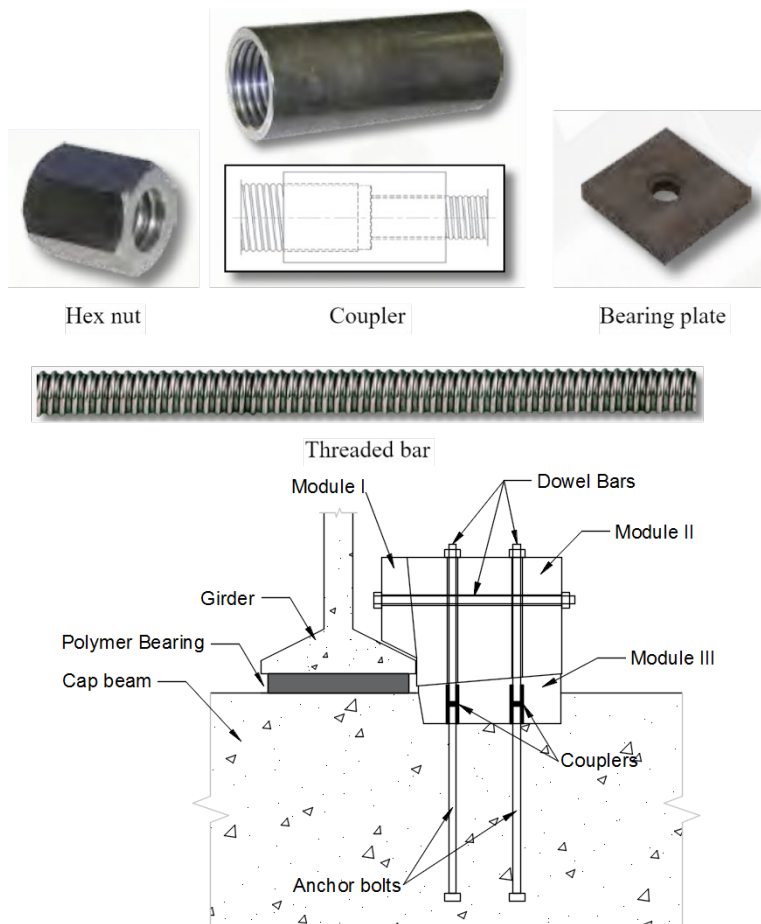
Figure 2.12 SMART shear key installation accessories

Chapter 3 Experimental Study of SMART Shear Keys

3.1 Loading setup

The loading device is a self-sustained test frame of which the maximal loading capacity is 4450 kN (1000 kips), as shown in Figure 3.1. The test frame includes two exterior rigid beams which are connected using six 35 mm (1-3/8 in) diameter Grade 150 Dywidag bars. To apply a load on each specimen, a movable rigid beam sandwiched between four top and bottom rollers and guided by a rail track was used to ensure unidirectional movement of the movable rigid beam. Two 2225 kN (500 kips) hydraulic cylinders were set between the exterior fixed red beam and the movable black beam so that the movable beam can apply a horizontal load on the test specimen in the middle of the test frame. Figure 3.1 shows an H-pile loaded axially. The details of the test frame are referred to Abdulazeez *et al.* (2019) and Ramadan and ElGawady (2019). In this study the SMART shear keys were loaded horizontally to investigate their resistance mechanism. The vertical resistance mechanism of concrete Module I was similar to the horizontal mechanism and thus studied through numeral simulations only.
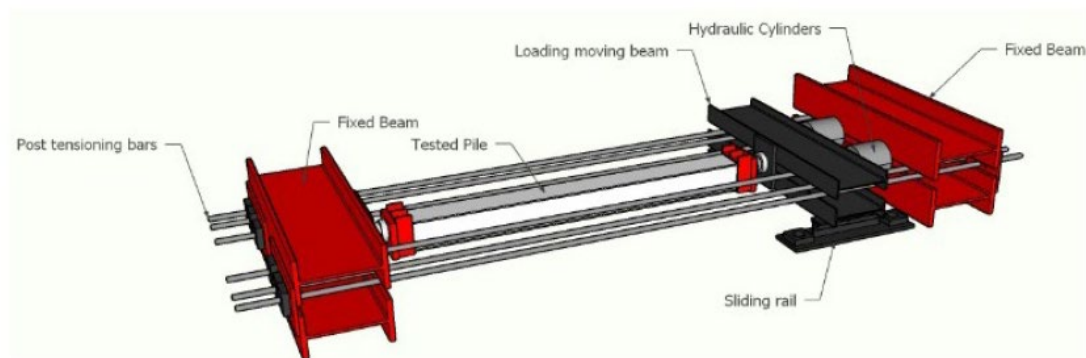
Figure 3.13 Test setup (Abdulazeez *et al.*, 2019)

<u>3.2 Concrete base</u>

In practice, the SMART shear key is installed on a bridge abutment or a bridge cap beam. To simulate this application scenario, a concrete base was designed to support the SMART shear key. Two design options for the concrete base were compared experimentally to determine a reliable way to test multiple shear key specimens consecutively. Besides, the concrete base can help the SMART shear key specimens fit into the test frame in Figure 3.1.

3.2.1 Trial concrete base

The first trial concrete base design is shown in Figure 3.2. The whole base is 1.5 m (5 ft) long, 0.6 m (2 ft) wide, and 0.5 m (1-3/4 ft) and 0.2 m (8 in) high at two ends. Details of the trial concrete design can be found in Appendix A. Figure 3.3 shows the casting of the first concrete base. The 28-day compressive strength of the concrete is 48 MPa (7 ksi). The top surface of the first concrete base is shown in Figure 3.4. The two couplers are cast into the concrete base and there is a pit preserved to hold concrete Module III. Concrete Module II is placed on top of Module III. The dowel bars connect the shear key and the base together.
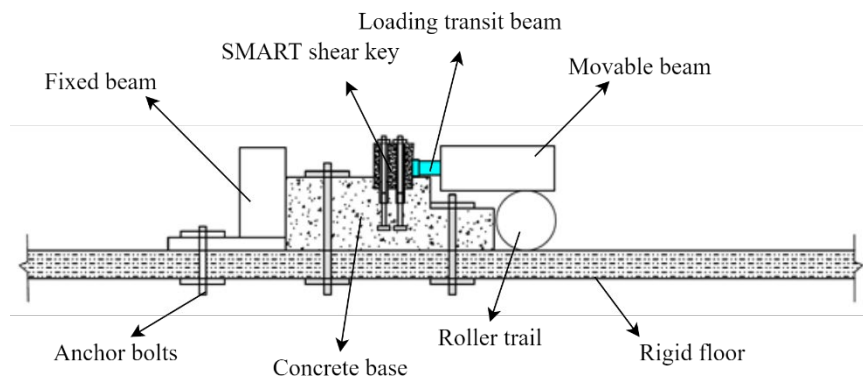
Figure 3.14 Trial concrete base
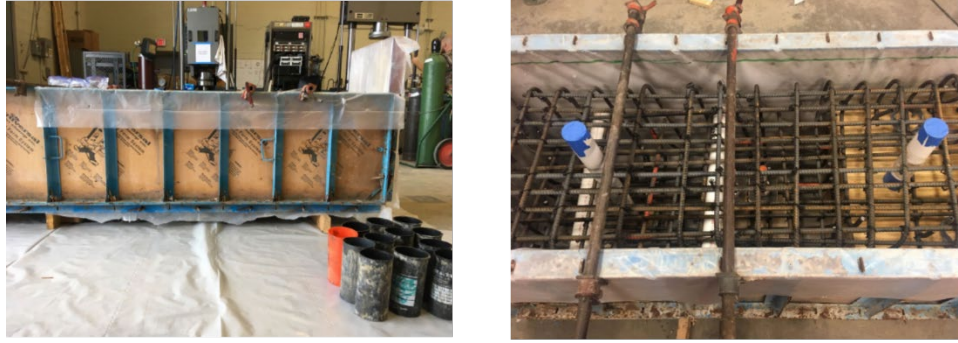
Figure 3.15 Casting of the first trial base
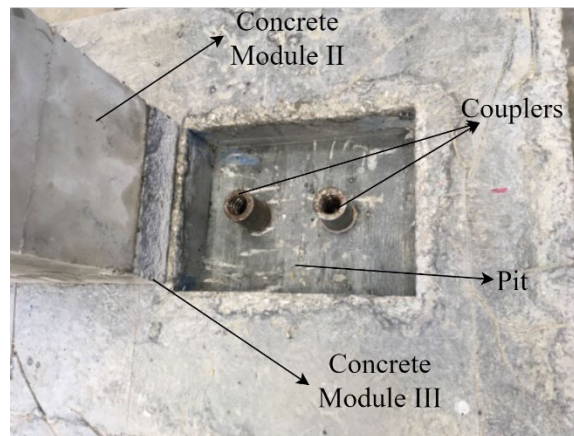
Figure 3.16 The first concrete base cast

3.2.2 Second concrete base

The second concrete base design is shown in Figure 3.5. The dimension of the whole

base is the same with the first base. Details of the second concrete design can be found in

Appendix A. The 28-day concrete compressive strength is 60 MPa (8.8 ksi). Figure 3.6 shows

the inside of the second concrete base. The main difference of the second concrete base from the

first concrete base is the couplers of the second base are not cast into the base. Instead, two steel

pipes are used to create two holes through the base to install the dowel bars and anchor the shear

keys. The top and bottom surfaces of the second concrete base are shown in Figure 3.7. There is

a pit on the top surface and the bottom surface, respectively. The pit on the top surface is to hold the SMART shear key Module III and the pit at the bottom is to hold the external anchors of the shear key. Unlike the first concrete base, the two couplers with the dowel bars of the second base can be replaced if necessary.
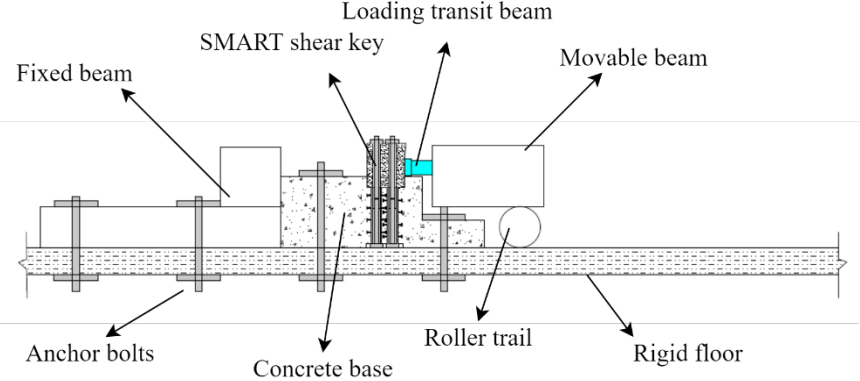
Figure 3.17 Second concrete base

Figure 3.18 Inside of the second concrete base

(a) Top surface

(b) Bottom surface

(c) Top surface with dowel bar and coupler

(d) Bottom surface with dowel bar
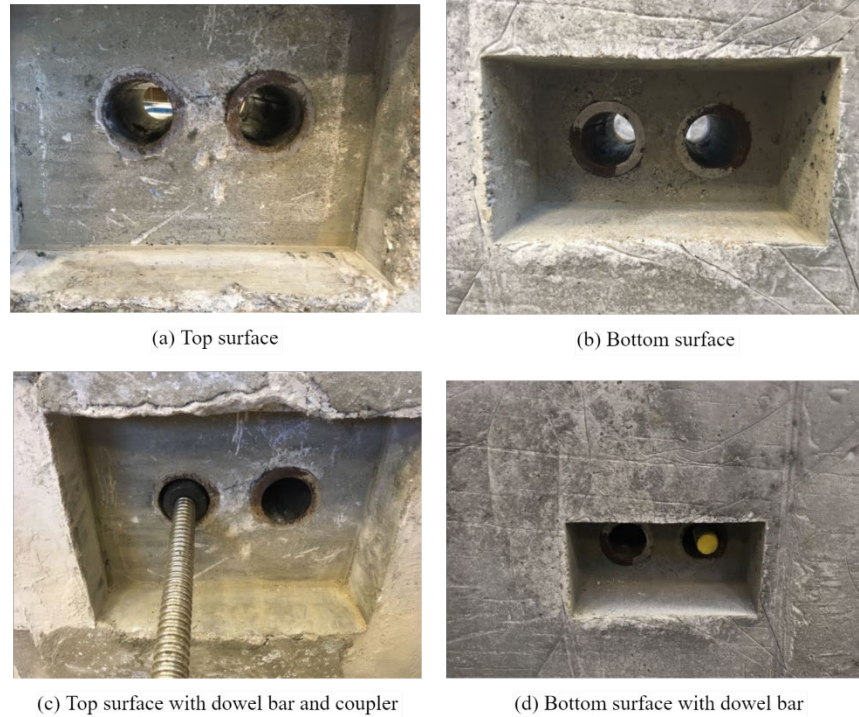
Figure 3.19 Top and bottom surfaces of the second concrete base

3.3 Loading test

The loading setup on a SMART shear key is presented in Figure 3.8. The SMART shear key was rested on top of the concrete base and loaded horizontally via a transfer loading beam. The load was applied monotonically at a rate of approximately 30 kN/min (6.7 kip/min) by two 2225 kN (500 kips) hydraulic jacks controlled manually by an oil pump. Each specimen was tested until it started to fail and became unstable. In totality, seven SMART shear keys were tested on the two concrete bases.
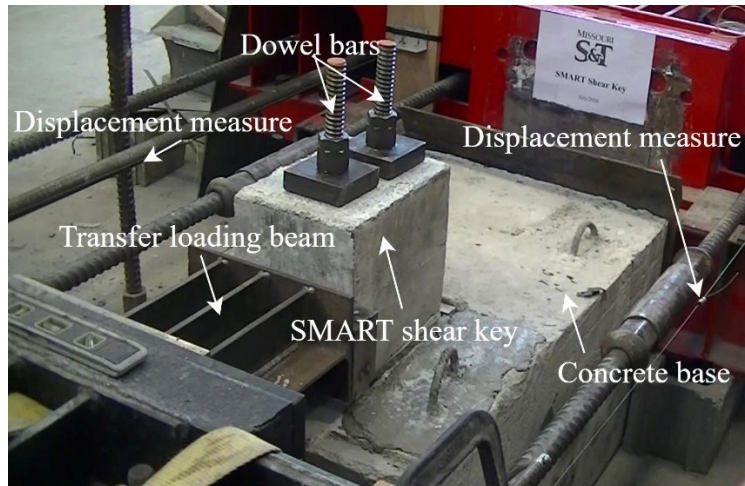
Figure 3.20 Loading test setup with a SMART shear key installed

3.3.1 Damage of concrete bases

Figure 3.9 shows the conditions of the two concrete bases at the completion of shear key tests. The first concrete base was used to hold the first SMART shear key containing 1-in long steel fibers. It can be seen from Figure 3.9(a, b) that the couplers were bent and punched through the shear key Module III. One of the couplers was broken after the Module III had been removed. Therefore, the first concrete base cannot be reused to test the remaining SMART shear keys. Figure 3.9(c) shows the couplers of the second base after shear key testing. The couplers remained intact and the bent dowel bars can be replaced for further tests. Therefore, the second base can be reused to test the following SMART shear keys.

(a) First concrete base

(b) Broken couple in first base

(c) Second concrete base

Figure 3.21 Damage on two concrete bases

3.3.2 Damage of installation accessories

Figure 3.10 shows the installation accessories after the loading test of the seven SMART shear keys. The hex nuts, bearing plates, and couplers all remained intact while the dowel bars were kinked as expected. However, the dowel bars did not fracture or fail during the tests.
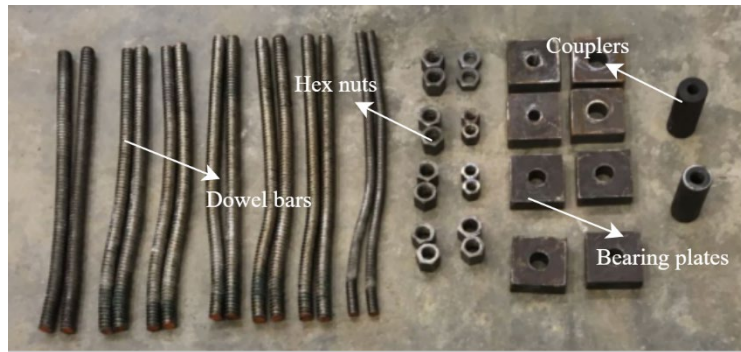
Figure 3.22 Installation accessories after loading tests

3.3.3 Concrete modules

Figure 3.11 shows the damage of SMART shear key concrete modules from different perspectives. It can be seen from Figure 3.11(f) that concrete Module II experienced splitting cracks because the dowel bars pushed against the concrete, while concrete Module III was locally crushed where the dowel bars were in contact with Module III on the sliding interface. Module III was not split into two parts because it was confined by the pit on the base. On the contrary, Module II was not confined and thus subjected to concrete splitting both on the front and back sides as the dowel action from the bar became effective. Note from Figure 3.11(f) that some Module IIs are split into two parts while others still hold together while displaying deep cracks.

(a) Front   (b) Side   (c) Top   (d) Back   (e) Inside
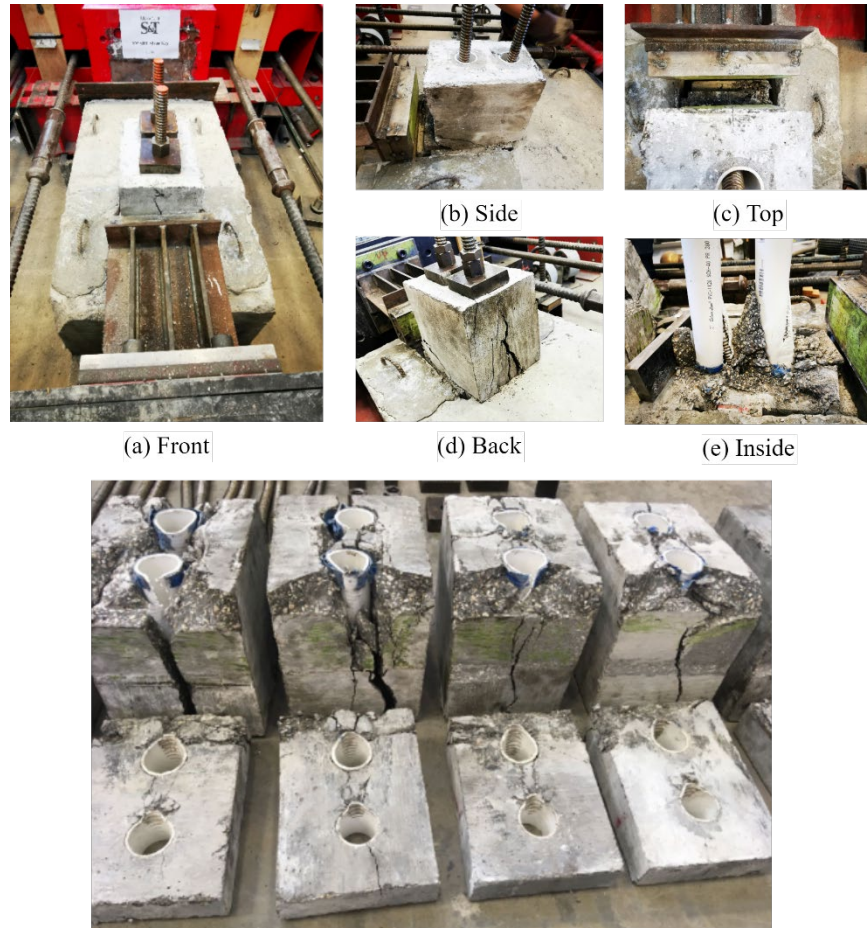
(f) Splitting cracks in Module II and sliding interface between Modules II and III

Figure 3.23 Failure modes of SMART shear keys

Figure 3.12(a) shows the concrete damage of modules in the seven tested SMART shear keys. The modules of the first tested shear key containing 1-inch steel fibers have no splitting cracks on the front and back side while the modules of shear keys including micro steel fibers all have severe cracks. Figure 3.12(b) and (c) compare the performance of the 1-inch steel fibers and micro steel fibers to hold the concrete. The longer steel fibers bridged the crack and held the concrete module together while the shorter steel fibers were completely pulled out of concrete. Therefore, the longer steel fibers could improve the ductility of the concrete modules.
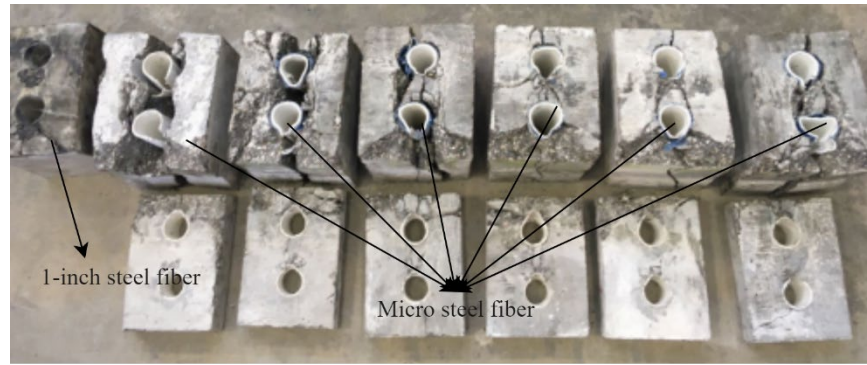
(a) concrete modules of seven SMART shear keys
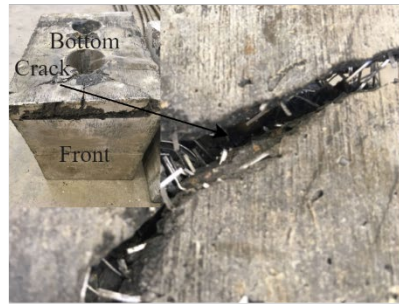
(b) 1-inch steel fibers

(c) micro steel fibers

Figure 3.24 Size effect of steel fibers

3.3.4 force-displacement curves

Figure 3.13 shows the force-displacement curves of the seven tested SMART shear keys. SMART Shear Key 0 is the shear key tested on the trial concrete base. SMART Shear Key 1-6 are installed and tested on the second concrete base. It can be seen from Figure 3.13 that the force-displacement curves of the seven SMART shear keys share a general trend but vary in terms of the sliding distance and maximum load-carrying capacity. These variations are mainly influenced by uncertain factors in the process of loading test, which will be investigated in detail in the following sections.
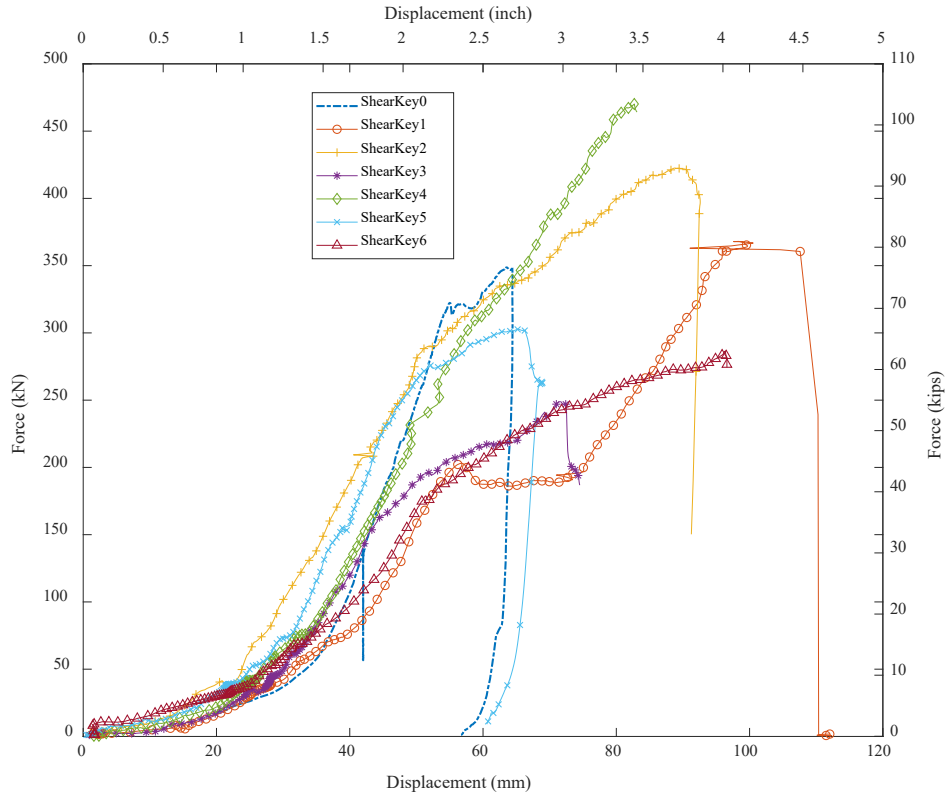
Figure 3.25 Force-displacement curves of seven SMART shear keys

3.3.4.1 SMART Shear Key 0

The loading of SMART Shear Key 0 stops at 350 kN (78.7 kips), 63.5 mm (2.5 in). The shear key fails soon after its dowel bars yield. The main reason for this failure is that one coupler on the trial base was broken, as shown in Figure 3.9(b). As a result, the concrete Module II of the shear key is subjected to only local cracks on the sliding interface.

3.3.4.2 SMART Shear Key 1

The loading of SMART Shear Key 1 stopped at the 368 kN (82.7 kips), 99.1mm (3.9 in). There is a plateau of the curve at the range of 57 mm (2.2 in) to 77 mm (3.0 in). One possible explanation for the plateau is that the concrete module is split suddenly to some depth so that the sliding distance increases while the loading force does not.

3.3.4.3 SMART Shear Key 2

The loading of SMART Shear Key 2 stops at 422 kN (95 kips), 91.5 mm (3.6 in). Shear

Key 2 has a higher maximum load-carrying capacity than Shear Key 1. After examining the

recorded video further, it is found that the shear key Module II is in contact with the concrete

base when Module II slides, as shown in Figure 3.14. The contact between the shear key and

base provides an extra resistant force to prevent Module II from sliding.

Figure 3.26 Restraint of Module II movement by the base

3.3.4.4 SMART Shear Key 3

The loading of SMART Shear Key 3 stops at 249 kN (56 kips), 72.5 mm (2.8 in). The

shear key has the lowest maximum load-carrying capacity among all the shear keys. The

deformation of the two dowel bars in SMART Shear Key 3 is shown in Figure 3.10 and Figure

3.15. The second dowel bar has a slight deformation, likely because it is not fully post-tensioned

since the dowel bars of all shear keys are hand-tightened. When the shear key is pushed, the

second bar does not bear much of the loading. Thus, the maximum load-carrying capacity of this shear key is lowest compared with other shear keys.

Figure 3.27 Deformation of the dowel bars in SMART Shear Key 3

3.3.4.5 SMART Shear Key 4

The loading of SMART Shear Key 4 stops at 470 kN (105.6 kips), 91.5 mm (3.3 in). The shear key has the highest maximum load-carrying capacity among all the shear keys. Like the SMART Shear Key 2, the shear key Module II contacts the concrete base when Module II slides, as shown in Figure 3.14. The contact between the shear key and base provides an extra resistant force to prevent Module II from sliding.

3.3.4.6 SMART Shear Key 5

The loading of SMART Shear Key 5 stops at the 303 kN (68 kips), 64.2 mm (2.5 in). The shear key has the second lowest maximum load-carrying capacity among all shear keys. The deformation of the dowel bars in Shear Key 5 is shown in Figure 3.10 and Figure 3.16. Like the Shear Key 3, the second dowel bar may not be fully post-tensioned. When the shear key is pushed, the second bar does not bear much of the loading. Thus, the maximum load-carrying capacity of this shear key is lower than all the others except Shear Key 3.

Figure 3.28 Deformation of the dowel bars in SMART Shear Key 5

3.3.4.7 SMART Shear Key 6

The dowel bars of SMART Shear Keys 0-5 have a diameter of 25 mm (1in). However, SMART Shear Key 6 is installed with dowel bars that have a diameter of 19 mm (3/4 in), shown in Figure 3.17. The loading of SMART Shear Key 6 stops at 286 kN (64 kips) and 99.3 mm (3.9 in).
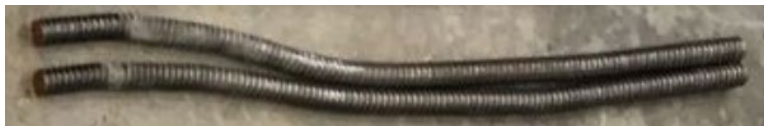
Figure 3.29 Deformation of the dowel bars in SMART Shear Key 6

3.4 Conclusions of the loading test results

Based on the discussion above, several conclusions can be drawn from the loading tests of the seven SMART shear keys:

(1) The maximum load-carrying capacity of the SMART shear keys varies from 249 kN (56 kips) to 470 kN (105.6 kips) due to the installation errors and dowel bar sizes. Similarly, the sliding distance of the SMART shear keys also varies from 64 mm (2.5 in) to 99 mm (3.9 in) due to uncertainties of the material strength, fiber distribution, etc., which might influence the ductility of the SMART shear keys.

(2) Generally, the SMART shear keys with 25 mm (1 in) dowel bars have an average resistant capacity of 360 kN (81 kips). The SMART shear key with a 19 mm (1in) dowel bar has a resistant capacity of 286 kN (64 kips). The resistant force of the SMART shear key is very close to the highest capacity, 348 kN (78.2 kips), of the resilient interior shear keys in Han *et al.* (2018, 2020). The sliding distances of SMART shear keys are generally longer than the resilient interior shear keys, 49.4 mm (1.9 in). The test results show that the proposed SMART shear keys can have an equivalent protection effect to the traditional resilient interior shear keys while having better ductility capacity.

(3) The resistant mechanism of the proposed SMART shear keys can be divided into three phases: Adaptive Phase, 0 – 20 mm (0 – ¾ in); Resistant Phase, 20 – 50mm (3/4 – 2 in); and Yielding and Failing Phase, beyond 50 mm (2in). The Adaptive Phase is mainly for the SMART shear keys to close the installation gaps. The Resistant Phase is when the SMART shear key in tightened. The dowel bars start to deform and contact the concrete. The Yielding and Failing Phase is when the dowel bars start to yield while the concrete generates deep splitting cracks.

(4) The experimental results show the failure mode of the SMART shear key is when the concrete modules are splitting and lose the ability to hold the dowel bars. The dowel bars will yield but not fracture.

(5) The concrete base used in this test does not damage after SMART shear keys fail. The failed SMART shear key is easily replaced with new ones equipped with new dowel bars. The test proves an easy replacement of the SMART shear key, which could improve the resilience of the whole bridge.

Chapter 4 Numerical and Analytical Studies of SMART Shear Keys

The experimental results show SMART shear keys have an equivalent load-carrying capacity to the resilient interior shear keys tested in Han *et al.*, (2018, 2020). In this chapter, the SMART shear keys are simulated both computationally and analytically to compare their load-carrying capacity.

4.1 Numerical simulation of SMART shear keys

4.1.1 ABAQUS simulation

The concrete modules II and III will be in contact with dowel bars as they slide against each other. The contact relation between the dowel bars and concrete is nonlinear. ABAQUS is a software tool for finite element analysis. The Explicit module in ABAQUS is very efficient to analyze highly nonlinear complex contact problems (ABAQUS, 2014). Therefore, the experiments of SMART shear keys are simulated in ABAQUS software. Only the shear keys without their concrete base are modeled with proper boundary conditions to save computing time.

4.1.1.1 Material properties

The SMART shear keys consist of two types of materials: steel and concrete. The experimental results show that the steel bars deformed but did not fracture. To capture its nonlinearity, steel is modeled with an elastic-perfectly plastic material law given the grade of the threaded bars, 517 MPa (75 ksi). According to the experimental results, the failure mode of concrete modules is mainly the splitting cracks on the front and back side of concrete Module II and the crushing where dowel bars are in contact with Module III. To capture the compressive and tensile failure in concrete modules, the concrete damaged plasticity (CDP) material law is used to model the concrete in ABAQUS, as shown in Figure 4.1. The main advantage of CDP is

that d_t (tension) and d_c (compression) take the stiffness degradation of concrete into account. The underlying theory of the CDP material law is referred to Lubliner *et al.* (1989) and Lee and Fenves (1998).
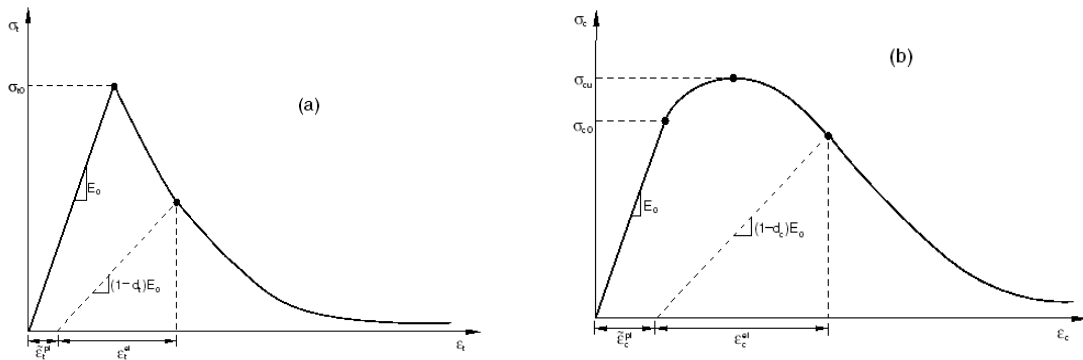
Figure 4.30 Concrete response to uniaxial loading in tension (a) and compression (b)

(ABAQUS, 2014)

4.1.1.2 Contact

The simulation of the SMART shear keys involves contact between different components like the bearing plates and concrete modules, dowel bars and concrete modules, concrete Module II and III, etc. In the case of the dowel bars and concrete modules, a force normal to the contacting surfaces acts on the dowel bars and the concrete modules when they are in contact with each other. In the case of concrete Module II and Module III, there is friction between the surfaces, such that shear forces are created to resist the sliding of the bodies. The general goal of contact simulations is to find the contact areas and calculate the contact pressures.

4.1.1.3 ABAQUS/Explicit and quasi-static analysis

ABAQUS/Standard (implicit) and ABAQUS/Explicit can solve a wide variety of problems. The SMART shear keys are loaded horizontally and slowly, which is considered a

typical quasi-static problem. ABAQUS/Explicit is chosen in this study because the Explicit

method is more readily available in solving certain types of static problems than the

ABAQUS/Standard. One advantage of the explicit procedure is the greater ease to resolve

complicated contact problems (ABAQUS, 2014). To apply the explicit method to quasi-static

problems, some special considerations are required. A static solution is always a long-time

solution which is computationally impractical in its natural time scale. Therefore, to obtain an

economical solution, the explicit analysis should model the process in a short time without taking

inertial forces into account.

Figure 4.2 shows the computational model in ABAQUS of SMART shear keys. The

dimension of the computational model is the same in Figure 2.8. The global general

("automatic") contact algorithm in ABAQUS/Explicit is used to allow fewer restrictions on the

types of involved surfaces. Particularly, a friction model is defined on the sliding interface as

shown in Equation 4.1

$$\tau_{\text{crit}} = \mu p \qquad (4.8)$$

where μ is the coefficient of the friction and p is the concrete pressure between the bottom of

Module II and the top of Module III. The coefficient μ is 0.41 based on experimental results.
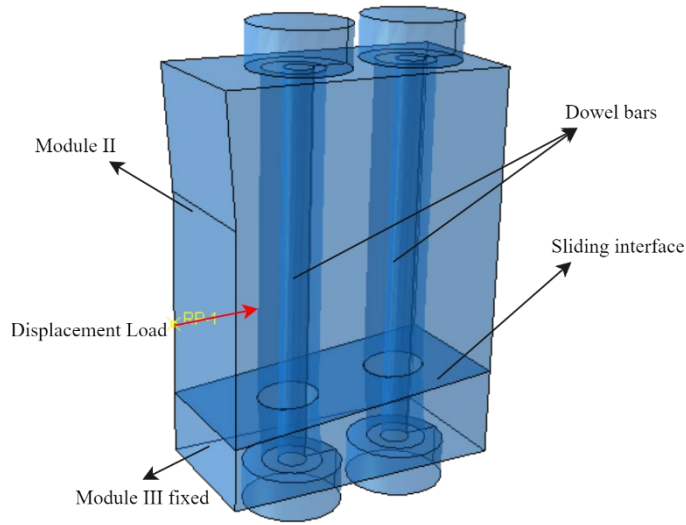
**Figure 4.31** ABAQUS computational model of the SMART shear key

4.1.2 Results

The compression and tension damage of components are calculated from the computational model. Figure 4.3 shows the compression damage of Concrete Module II. When compressed by the dowel bars, the concrete is severely damaged by compression, which agrees with the experimental observation in Figure 3.11(f) and Figure 3.12(a). Figure 4.4 shows the tension damage of Concrete Module II. When in contact with the dowel bars, the concrete at its bottom corner suffers the most severe tension damage, which also matches the experimental result in Figure 3.11(f) and Figure 3.12(a). Besides, the back side of Concrete Module II generates a long crack in Figure 3.11(d), which is also observed in the left figure of Figure 4.4. Figure 4.5 shows the concrete damage of Module III, which matches the experimental result in Figure 3.11(f) and Figure 3.12(a). Figure 4.6 shows the stress of the dowel bars. The deformation of dowel bars matches the experimental results in Figure 3.10. The numerical simulation result of the concrete damage is validated by the experimental results. The numerical simulation predicts

an ultimate resistant force of 385 kN of SMART shear keys with 25-mm dowel bars and 232 kN of SMART shear keys with 19-mm dowel bars. The numerical simulation might underestimate the load-carrying capacity because of the stiffness degradation of the CDP concrete model.
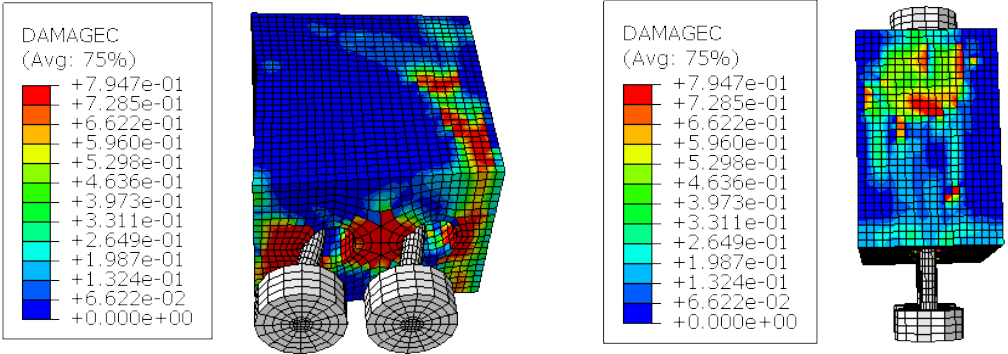
Figure 4.32 Compression damage of Concrete Module II from bottom (left) and back (right) sides
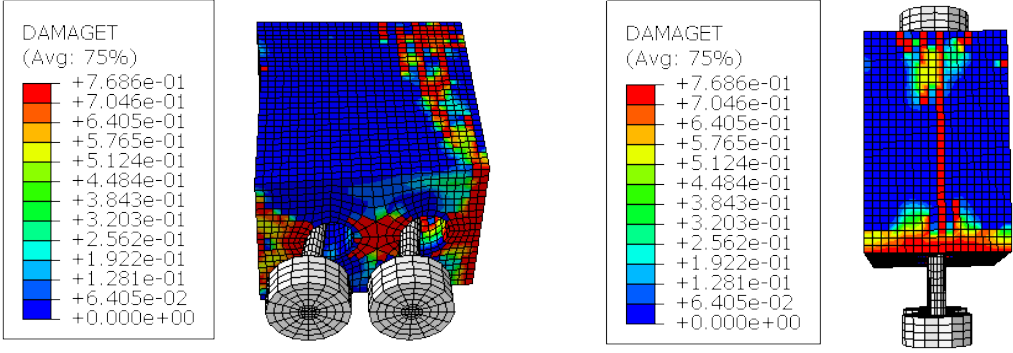
Figure 4.33 Tension damage of Concrete Module II from bottom (left) and back (right) sides
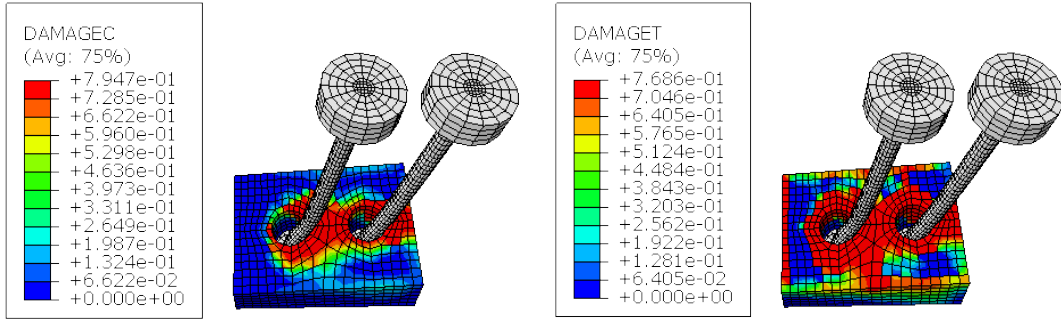
Figure 4.34 Compression damage from bottom (left) and tension damage from the back (right)

of Concrete Module III
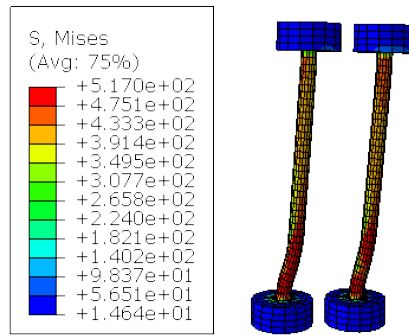
Figure 4.35 Stress of dowel bars

4.2 Theoretical analysis of SMART shear keys

The ultimate capacity of the SMART shear keys depends on the flexural behavior of the

vertical dowel bars and the friction of the sliding interface. It can be derived from the force

balance of concrete Module II in Figure 4.7. The sliding shear mechanism of SMART shear keys

is very similar to that of the resilient interior shear key in Han *et al.* (2018, 2020). The main

difference is that the sliding interface of SMART shear keys has an angle α. Similarly, the

maximal capacity of the SMART shear key can be calculated from Equation 4.2

$$H = (2T) \left(\frac{\mu \cos \alpha + \sin \alpha}{\mu \sin \alpha + \cos \alpha} \cos \beta + \sin \beta \right) \qquad (4.9)$$

where $\cos \beta = \frac{1}{1+\varepsilon_m}$, $\sin \beta = \frac{\sqrt{\varepsilon_m^2 + 2\varepsilon_m}}{1+\varepsilon_m}$, $\varepsilon_m = 0.005$ is the ultimate strain of the steel dowel bar, α

$= 5°$, $\mu = 0.41$, $2T = A_s f_m$, A_s is the total area of the vertical dowel bars, and f_m is the ultimate

tensile strength of vertical dowel bars. Therefore, Equation 4.2 can be transformed into Equation

4.3, which is very similar to Equation 2.3 of interior resilient shear keys, except the effect of the

angle of the sliding interface. However, the experimental results as shown in Figure 3.10 indicate

different deformations in the dowel bars of a shear key. Therefore, Equation (4.3) can be

modified to account for different behavior in two dowel bars as expressed in Equation (4.5).

$$H = (A_s f_m) \left(\frac{\mu + \tan \alpha}{1 + \mu \tan \alpha} \frac{1}{1 + \varepsilon_m} + \frac{\sqrt{\varepsilon_m^2 + 2\varepsilon_m}}{1 + \varepsilon_m} \right) \qquad (4.10)$$

$$\tan (\beta) = \frac{\delta l}{l} \qquad (4.11)$$
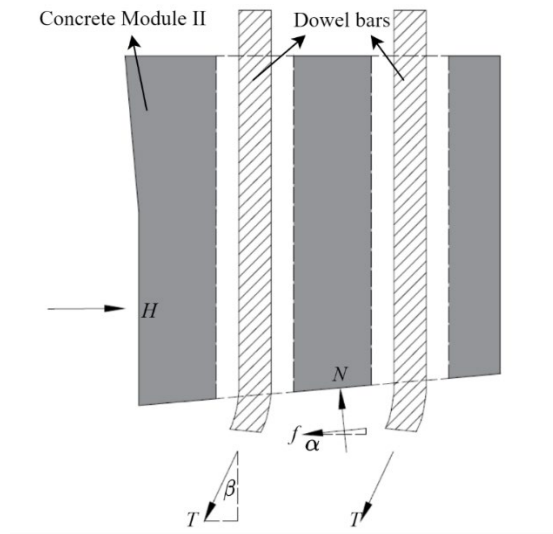
Figure 4.36 The sliding friction mechanism of SMART shear keys
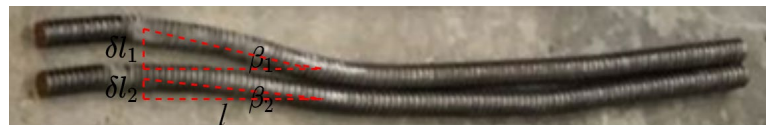
Figure 4.37 The kinking angle of the dowel bars

$$H = T_1 \left(\frac{\mu + \tan\alpha}{1 + \mu\tan\alpha} \cos\beta_1 + \sin\beta_1 \right) + T_2 \left(\frac{\mu + \tan\alpha}{1 + \mu\tan\alpha} \cos\beta_2 + \sin\beta_2 \right) \qquad (4.12)$$

In Figure 4.8, δl_1 and δl_2 are horizontal displacements of the two dowel bars, and l is the kinking length equal to 203 mm (8 in). The angles β_1 and β_2 can be calculated from Equation 4.4. When the yield strain ε of the steel dowel bars is 0.002, the kinking angle can be calculated from $\cos\beta = \frac{1}{1+\varepsilon}$. Furthermore, the corresponding threshold yield deformation of dowel bars is calculated as 13 mm (0.51 in) from Equation 4.4. Similarly, the ultimate strain of the steel dowel is 0.005. The corresponding threshold yield deformation of dowel bars is calculated as 20.3 mm

42

(0.8 in). According to the dowel bar properties, the yield force of the 25-mm dowel bars is 264 kN and the ultimate force is 351 kN. For 19-mm bars, the yield force is 147 kN and the ultimate force is 196 kN. Therefore, the dowel bar forces of the loaded shear keys can be obtained from interpolation, as shown in Figure 4.9.
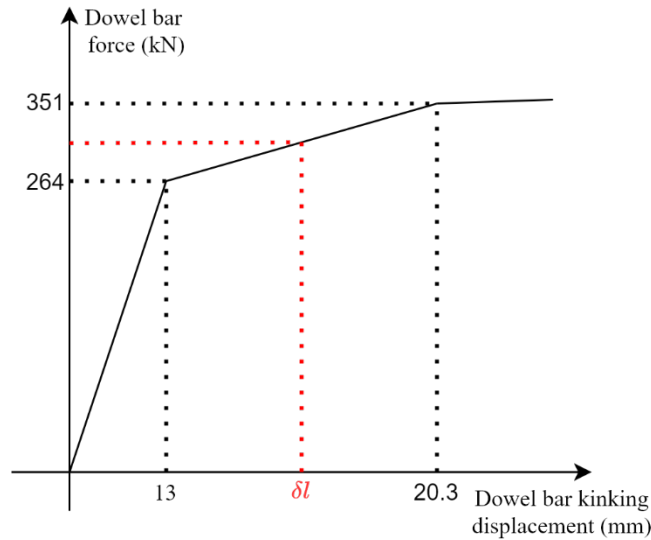
Figure 4.38 Dowel bar tension force interpolation

When the dowel bar forces and kinking angles are inputted into Equation 4.5, the theoretical load-carrying capacity of each SMART shear key can be calculated, as listed in Table 4.1. Table 4.1 demonstrates that the theoretical and experimental results are in good agreement. For the SMART Shear Key 4 with 25 mm (1 in) dowel bars and SMART Shear Key 6 with 19 mm (1 in) dowel bars, both dowel bars reach the ultimate forces. For SMART Shear Keys 1, 2, 3, and 5 with 25 mm (1 in) dowel bars, one dowel bar force does not reach the ultimate force and hence is obtained from interpolation from Figure 4.9. Particularly, Shear Key 3 and 5 have one dowel bar force significantly lower than the other dowel bar because the kinking displacement is very small. The probable reason is that these two dowel bars are fully post-tensioned when the

43

shear key is installed. When fully post-tensioned to reach their yield forces, the dowel bars are easily kinked as the concrete modules bcome in contact with the dowel bars, because the steel bars already yield. When not fully tensioned, it is difficult for the concrete module to kink the dowel bars because they remain elastic with limited deformation. Therefore, these two dowel bars do not develop large tension forces.

Table 4.2 Theoretical load-carrying capacities of SMART shear keys

Shear key #	δl_1 (mm)	δl_2 (mm)	T_1 (kN)	T_2 (kN)	Theory (kN)	Experiment (kN)	Error (kN/kN)
1	30.5	12.7	351	257	358	368	2.7%
2	43.2	17.8	351	321	419	422	0.7%
3	38.1	0	351	0	232	249	6.8%
4	53.3	25.4	351	351	463	470	1.5%
5	38.1	7.6	351	119	292	303	3.6%
6	76.2	38.1	196	196	285	286	0.4%

4.3 Conclusions

(1) Numerical simulation results validate the damage and failure modes of SMART shear keys observed during the experiment. The dowel bars are kinked but do not fracture when the SMART shear keys are loaded. However, concrete is crushed when in contact with the dowel bars. The concrete modules are split due to the pressure from bearing plates on the top. Therefore, the SMART shear keys will fail when the concrete modules lose their ability to hold the dowel bars.

(2) Theoretical analysis reveals the kinking angles of dowel bars dominate the maximal load-carrying capacity of SMART shear keys. The load-carrying capacity increases with the kinking angle. Theoretical results of the maximal load-carrying capacity are very close to those of the experimental results with the largest error being 6.8%.

Therefore, the theoretical equations can be used to evaluate the capacity of SMART shear keys in design.

(3) The SMART shear keys are proved to provide an equivalent load-carrying capacity with the existing resilient interior shear keys with the same sliding failure mechanism. However, the design of SMART shear keys can protect the bridge cap beams from damage and will be much easier to replace once the shear keys are damaged in moderate-to-large earthquake events, thus increasing the resilience of the bridge structure. More studies will be conducted to estimate the performance of SMART shear keys in bridges through seismic analysis.

References

AASHTO (2014). *LRFD Bridge Design Specification*, *American Association of State Highway and Transportation Officials (AASHTO)*, Washington DC.

ABAQUS (2014). 'ABAQUS 6.14', *Abaqus 6.14 Analysis User's Guide*.

Abdulazeez, M. M. *et al.* (2019). 'Behavior and repair of corroded steel H-piles Phase I (axial behavior),' Final Report, Mid-America Transportation Center.

Azizinamini, A. and Gull, J (2014). Proceedings of 2014 National Accelerated Bridge Construction Conference, December 4-5, 2014, Miami, Florida.

Bozorgzadeh, A. *et al.* (2006). 'Capacity evaluation of exterior sacrificial shear keys of bridge abutments', *Journal of Bridge Engineering*.

Chen, G. *et al.* (2005). 'Analysis of the Interstate 10 twin bridge's collapse during Hurricane Katrina,' *Science and the Storms: The USGS Response to the Hurricanes of*, pp. 35–42.

Chen, G. *et al.* (2010). '2010 Chile Earthquake implications to the seismic design of bridges,' in *Proceedings of the 26th US-Japan Bridge Engineering Workshop*, pp. 203–216.

Han, Q. *et al.* (2017). 'Seismic behavior of reinforced concrete sacrificial exterior shear keys of highway bridges,' *Engineering Structures*.

Han, Q. *et al.* (2018). 'Seismic performance of interior shear keys of highway bridges,' *ACI Structural Journal*.

Han, Q. *et al.* (2020). 'Seismic capacity evaluation of interior shear keys for highway bridges,' *Journal of Earthquake Engineering*.

Kottari, A., Benson Shing, P. and Bromenschenkel, R. (2020) 'Shear behavior of exterior non-isolated shear keys in bridge abutments,' *ACI Structural Journal*.

Lee, J. and Fenves, G. L. (1998). 'Plastic-damage model for cyclic loading of concrete structures,' *Journal of Engineering Mechanics*.

Lubliner, J. *et al.* (1989). 'A plastic-damage model for concrete,' *International Journal of Solids and Structures*.

Luna, R. *et al.* (2006). 'Reconnaissance Report of the Post-Katrina Hurricane Disaster,' NHMI-UMR-USGS File Report, University of Missouri-Rolla.

Megally, S. H., Silva, P. F. and Seible, F. (2002). 'Seismic response of sacrificial shear keys in bridge abutments,' *UCSD Report No. SSRP-2001/23*.

Ramadan, A. and ElGawady, M. A. (2019). 'Axial behavior of corroded H-Piles,' in *Proc., IABSE Congress*.

Silva, P. F., Megally, S. and Seible, F. (2003). 'Seismic performance of sacrificial interior shear keys,' *Structural Journal*, 100(2), pp. 177–187.

Silva, P. F., Megally, S. and Seible, F. (2009). 'Seismic performance of sacrificial exterior shear keys in bridge abutments,' *Earthquake Spectra*.

Silva, P. F. and Nguyen, T. L. T. (2010). 'Influence of shear key modeling on the performance of bridges under simulated seismic loads,' in *Bridge Maintenance, Safety, Management and Life-Cycle Optimization - Proceedings of the 5th International Conference on Bridge Maintenance, Safety and Management*.

Yen, W. H. P., Chen, G., Yashinsky, M., Hashash, Y., Holub, C., Wang, K., & Guo, X. (2011). *China Earthquake Reconnaissance Report: Performance of transportation structures during the May 12, 2008, M7. 9 Wenchuan earthquake,* Publication No. FHWA-HRT-11-029, Federal Highway Administration.

Yen, W.-H. P. *et al.* (2011). *Post-earthquake Reconnaissance Report on Transportation Infrastructure Impact of the February 27, 2010, Offshore Maule Earthquake in Chile*, Publication No. FHWA-HRT-11-030, Federal Highway Administration.

Yen, W. P. *et al.* (2009). 'Lessons in bridge damage learned from the Wenchuan earthquake,' *Earthquake Engineering and Engineering Vibration*.

Appendix A Extra Information of Concrete Base Design
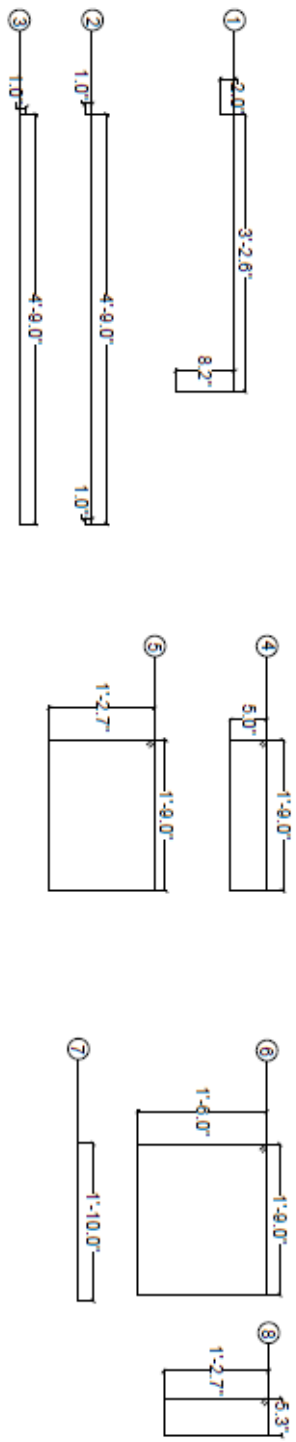
Rebar and stirrup details

Order	Type	Number	Single length (in)	Total length (ft-in)
①	#4 Rebar	8	52.10	34-9
②	#4 Rebar	8	59.00	39-4
③	#4 Rebar	8	59.00	39-4
④	#3 Stirrup	5	56.00	23-4
⑤	#3 Stirrup	4	75.40	25-2
⑥	#3 Stirrup	5	82.00	34-2
⑦	#3 Stirrup	9	22	16-6
⑧	#3 Stirrup	8	40	28-0

Note: 1. total # 4 rebar length is 113 ft 5 in;
2. total # 3 stirrup length is 117 ft 2 in;
3. hookup size unknown yet.

① 2'-0", 3'-2.6", 8.2"

② 1'-0", 4'-9.0", 1'-0"

③ 1'-0", 4'-9.0"

④ 5.0", 1'-9.0"

⑤ 1'-2.7", 1'-9.0"

⑥ 1'-6.0", 1'-9.0"

⑦ 1'-10.0"

⑧ 1'-2.7", 5.3"

49